Study of Weld Bead Geometry for GMAW Additive Manufacturing of Duplex Stainless Steel

Huifeng Wang
PhD Student
Charles Darwin University
Faculty of Science and Technology
Australia

Štefanija Klarić
Professor
Charles Darwin University
Faculty of Science and Technology
Australia

Sara Havrlišan
Assistant Professor
University of Slavonski Brod
Mechanical Engineering Faculty of Slavonski Brod
Croatia

The application of the Gas Metal Arc Welding (GMAW) Additive Manufacturing (AM) process for producing duplex stainless steel components can reduce material waste and enable control of the microstructure and alloy composition in different regions of the product through careful selection and adjustment of welding parameters. However, because achieving a higher deposition rate, greater reinforcement and penetration, and a narrower bead width must be balanced, simply setting welding parameters may not always yield the desired results. Therefore, the aim of this research is to analyze the effects of voltage, wire feed speed (WFS), and travel speed (TS) to determine their optimal values using experimental design methods. Grey Relational Analysis (GRA) was employed for multi-objective optimization, resulting in the following optimal parameters: voltage (16.783 V), WFS (403.231 cm/min), and TS (24.862 cm/min). These parameters were then applied to fabricate a 10-layer AM wall, achieving stable arc behavior, good interlayer bonding, and consistent wall morphology.

Keywords: *gas metal arc weld (GMAW), duplex stainless steel (DSS), additive manufacturing (AM), multi-objective optimization*

1. INTRODUCTION

Additive manufacturing (AM) - a layer-by-layer depo–sition process has rapidly developed in the last three decades [1-3]. It has many advantages, such as free design, less material wastage, and short lead time [4-7], which enables people to customize parts with complex contours and cavities without needing advanced design or development of expensive tooling. Both avoiding and reducing limitations of the shape and size in traditional manufacturing process can reduce the power consum–ption or the working hours and meet the manufacturing concept of modern product parts with near-net shape [8, 9]. AM is now widely recognized and gradually accep–ted. It has been used in the design, production, and deve–lopment of capital parts as well as technology-intensive industries such as aerospace, medical, automotive, and instrumentation [10-12]. Another advantage of AM is to reduce the weight of parts, which can be employed through production of hollow structures [13, 14].GMAW Additive Manufacturing is a type of Wire arc additive manufacturing (WAAM), which can manu–facture pro–ducts through the accumulation of melted/ joined metallic materials [15, 16]. Besides mentioned advantages of the AM process, GMAW AM could also manufacture large-scale products, with a higher depo–sition rate and lower cost compared to other AM methods [17].

Due to excellent mechanical and corrosive pro–perties, stainless steels have a wide range of appli–cations, such as automotive, medical, and engineering [18]. Duplex stainless steel (DSS) is a special kind of stainless steel with an equal ratio of ferrite (α) and aus–tenite (γ) phases, leading to enhanced strength, imp–roved weldability, higher toughness, and better cor–rosion resistance [19].

The requirements of weld bead for the AM process are different from the normal welding joints because the accumulation speed and product shape require more awareness compared with the welding joints. Therefore, the welding parameters would be determined based on the AM process features. Although numerous studies [19-27] have investigated wire arc additive manu–facturing (WAAM) of DSS/SDSS-focusing on aspects such as thermal cycles, microstructure evolution, and corrosion behavior- the welding wires, substrates, and process conditions used in those works differ from those in the present study. As a result, their parameter sets cannot be directly adopted; however, the reported para–meter ranges provide useful references for selecting suitable experimental parameters in this research.

As per the Table 1, the voltage range for DSS/SDSS is about 16-25 V, the WFS is around 300-600 cm/min and the TS is about 12-30 cm/min. To determine the suitable welding parameters for this study, the welding parameters will range: voltage from 16-21 V, the WFS from 400-600 cm/min, and the TS from 15-25 cm/min .

During the AM process, to obtain effective depo–sition speed, a higher manufacturing speed, higher bead height (reinforcement), and a lower width should be considered [28]. To develop the suitable parameters, design experiment methods, Analysis of variance (ANOVA), and some optimization algorithms can be utilized. For example, Surface Methodology (RSM) and Taguchi method were applied to analyze the design matrix to obtain the response functions including bead height (H) and bead width (W) [29].

Received: June 2025, Accepted: July 2025
Correspondence to: Huifeng Wang, PhD Student
Charles Darwin University, Faculty of Science and Technology, Darwin, Australia
E-mail: huifeng.wang@students.cdu.edu.au
doi: 10.5937/fme2503471W

Table 1. Welding parameters for DSS/SDSS utilized in the AM process

Materials	Substrate	Voltage (V)	Current (A)	WFS (cm/min)	TS (cm/min)	Author and Ref.
ER2594	Q345	19	-	500	24	Huang et al. [20]
ER2594	AISI 2507	16.2	140	300	-	Kannan et al. [21, 22]
E2209T0–4/1	Q345	25	187	-	28.2	Y. Zhang et al. [23]
ER2594	Mild steel	20-30	-	200-600	33.3-66.7	Kumar, P. and K. Maji [24]
ER 2209	UNS S32205	16.2-17.9	145-185	400-520	25.8	A. F. Miranda-Pérez et al. [25]
2209	2205	24.5	147	-	39	Hosseini, V. A. et al. [19]
DSS flux-cored wire	Q345	30	145		32.4	Zhang et al. [26]
2205	Grade 304	17	-	386	25-27	Nikola K. A. et al. [27]

Figure 1. Welding robot system in the experiment

Although previous studies have addressed WAAM of stainless steels, the detailed influence of welding parameters on weld bead geometry-such as reinfor–cement, bead width, reinforcement-to-width ratio, and penetration not been fully explored. Moreover, due to differences in materials and process conditions, existing parameter sets are not directly applicable. This study investigates how key process parameters affect bead geometry for a specific material combination, providing insights for process control and optimization in WAAM.

The introduction of optimization algorithms is usually due to that a certain parameter, such as WFS, responds to weld width and weld height in opposite ways. In order to ensure the desired results, multi-optimization was required [30].

In literacy,the multi-objective grey wolf algorithm [30], teaching-learning-based optimization (MOTLBO) [31], heat transfer search (HTS) algorithm [32], and Grey relational analysis (GRA) [33] were all employed for this kind of optimization.

In this paper, bead-on-plate for DSS using GMAW AM process is employed by considering welding parameters such as V, WFS, and TS. R, W, R/W, and penetration (P) will be treated as the responses. The specific process is as follows: first, the Box-Behnken design (BBD) is used to design the experimental scheme to reasonably arrange the experiment and collect data; then the response surface methodology (RSM) is used to model the experimental data, and the significance of each factor on the response variable is evaluated through analysis of variance (ANOVA) to identify the key influencing factors; then, grey relational analysis (GRA) is performed based on the experimental data to achieve multi-objective optimization, calculate the grey relational degree of each experimental scheme and screen out the optimal process parameters; finally, the selected optimal scheme is experimentally verified to ensure the feasibility and reliability of the optimization results.

The results of this study are expected to support process optimization and quality control in WAAM applications involving duplex stainless steels. This is particularly relevant in industries such as offshore engineering, chemical processing, and structural fabrication where consistent weld bead geometry and layer quality are critical for reliable component performance.

2. MATERIALS AND EQUIPMENT

The present study, bead-on-plate trials, will be carried out on a 316L stainless steel plate (100 × 50 × 5 mm) utilizing a 1.2 mm diameter ER2209 metal core wire. The substrate plate should be kept clean and dry before welding.

The experimental setup involves a FANUC Robot, R-30iB robot control cabinet, wire feeder, Lincoln welding power, and shielding gas cylinders (argon), shown in Figure 1. The GMAW torch is installed in front of the robot arm to complete the welding process.

100% Argon is employed for the product shield gas and the gas flow is 15 L/min [24, 34]. Welding voltages, WFS, and TS are considered as the independent variables. The wire feed speed range is 400-600 cm/min, and the travel speed range is 15-25 cm/min, as mentioned in the introduction and shown in Table 2.

Table 2. The GMAW process parameters

Parameters	Unit	Value
Voltage	V	16, 18.5, 21
WFS	cm/min	400, 500, 600
TS	cm/min	15, 20, 25
Gas flow rate	L/min	15

Welding bead geometry is measured using a Vernier caliper. The bead geometry includes bead reinforcement (R) and bead width (W), the R/W ratio and penetration (P) .

3. METHODOLOGIES

3.1 RSM and BBD

Response surface methodology (RSM) is a modeling and analysis method based on mathematics and statistics, which is used to study the impact of multiple variables on the response variable and find the optimal conditions. It is usually used to fit regression models and analyze response surfaces after obtaining experimental results [35-37]. Box-Behnken design (BBD) is a common experimental design method, often used in conjunction with RSM. BBD can effectively reduce the number of experiments and evaluate the interaction between variables without involving extreme combinations [38-40]. For the case of three factors and three levels, 15 experiments can be designed using BBD (as shown in Table 3), which greatly reduces the workload compared to the 27 experiments of full factorial design.

Table 3. Experimental Plan using Box-Behnken Design for ER2209 GMAW

Run order	Voltage (volts)	WFS (cm/min)	TS (cm/min)
1	3 (21)	1 (400)	2 (20)
2	2 (18.5)	2 (500)	2 (20)
3	2 (18.5)	3 (600)	1 (15)
4	2 (18.5)	2 (500)	2 (20)
5	1 (16)	1 (400)	2 (20)
6	2 (18.5)	2 (500)	2 (20)
7	1 (16)	3 (600)	2 (20)
8	3 (21)	2 (500)	3 (25)
9	3 (21)	2 (500)	1 (15)
10	1 (16)	2 (500)	1 (15)
11	3 (21)	3 (600)	2 (20)
12	1 (16)	2 (500)	3 (25)
13	2 (18.5)	1 (400)	1 (15)
14	2 (18.5)	3 (600)	3 (25)
15	2 (18.5)	1 (400)	3 (25)

The RSM models expresses the responses using different parameters and can be displays in the form of equations. Thefour common model types in RSM are linear, 2F, Quadratic, and Cubic models. Its general equation is shown below (1), where β_0 is a constant coefficient, β_i stands for linear, β_{ii} is the quadratic terms and β_{ij} stands for cross-products of parameters. The choice of model will be based on the fitting statistics of Design expert 12. Through analysis and comparison, this paper mainly adopts the quadratic regression model (Quadratic Model).

$$Y = \beta_0 + \sum_{i=1}^{k} \beta_i x_i + \sum_{i=1}^{k} \beta_{ii} x_i^2 + \sum \sum_{i<j} \beta_{ij} x_i y_j + \varepsilon \qquad (1)$$

This study used analysis of variance (ANOVA) to evaluate the significance of each factor and its interaction term on the response variable to verify the validity of the regression model. Subsequently, the established regression model was used to generate 100 sets of prediction data with different parameter combinations, and the optimal solution was determined through grey relational analysis (GRA). The specific process is shown in the next section.

3.2 Grey relational analysis (GRA)

Grey relational analysis is applied in this study, which analyzes the relationship between different responses and provides a multi-objective optimization. As mentioned above, there are four responses to be analyzed, which are bead reinforcement (R), bead width (W), aspect ratio (R/W), and penetration (P). Among them, the larger R, R/W and P are better, while the smaller W is better. GRA can help to express the different requirements to a single requirement using the specific normalization process [30, 37].

Generally, there are three steps for the GRA process:

(1) Nomination and calculation of GRA for the experimental results [33]

According to different requirements of responses, there are two normalized equations, which are the smaller the better equation (2) and the larger the better equation (3).

$$x_{ij} = \frac{\max_j \left(y_{ij}\right) - y_{ij}}{\max_j \left(y_{ij}\right) - \min_j \left(y_{ij}\right)} \qquad (2)$$

$$x_{ij} = \frac{y_{ij} - \min\left(y_{ij}\right)}{\max_j \left(y_{ij}\right) - \min_j \left(y_{ij}\right)} \qquad (3)$$

where x_{ij} is the normalized results, and y_{ij} is the ith parameter in the jth experiment, $\max_j(y_{ij})$ and $\min_j(y_{ij})$ are the largest and smallest values of the ith parameter in all the solutions.

(2) The grey relational coefficient (GRC) calculation [33]

Grey relational coefficients, ξ_{ij}, are calculated to express the relationship between the ideal and the actual experimental results and can be expressed as:

$$\xi_{ij} = \frac{\min_i \min_j \left|x_i^0 - x_{ij}\right| + \zeta \max_i \max_j \left|x_i^0 - x_{ij}\right|}{\left|x_i^0 - x_{ij}\right| + \zeta \max_i \max_j \left|x_i^0 - x_{ij}\right|} \qquad (4)$$

where x_i^0 is the ideal normalized result (i.e., best-normalized result = 1) for the ith quality characteristics and ζ [0,1] is a distinguishing coefficient. Considering the importance of each response in future AM research,

the value of ζ is set to be 0.3, 0.2, 0.2, and 0.3, respectively, R, W, R/W, and P.

(3) The grey relational grade (GRG) calculation

The GRG corresponding to each performance characteristic is to be computed, and the overall evaluation of the multi-response characteristics is based on the GRG, which is given by:

$$GRG = \frac{1}{n}\left(\sum_{i=1}^{n} GRC\right) \tag{5}$$

All GRGs of the predicted solutions are compared, and the top three are selected as the optimal schemes for better welding bead geometry.

4. RESULTS AND DISCUSSION

The geometry of the weld bead is a set of parameters that is defined in the design stage and measured and controlled throughout the process to achieve the required quality [41]. Three values of the geometry are measured as shown in Figure 2, which are the bead width (W), bead reinforcement (R) and penetration (P). Additionally, the aspect ratio for R/W is calculated as the third response.

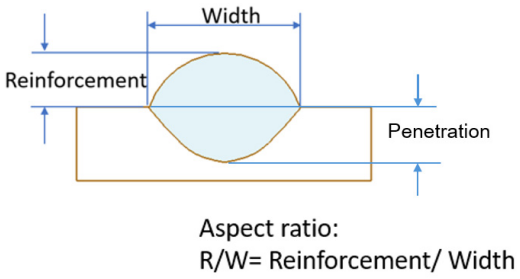

Figure 2. The geometry of a weld bead

4.1 Development of regression model equation

As shown in Table 4, three levels-three factors RSM-BBD was carried out, and 15 trials were welded as shown in Figure 3. During this process, a vernier caliper is employed to measure the R and W. Each experiment was repeated three times, and the average value of that was obtained for further analysis. Figure 3 displays the appearance of the specimens of single-bead deposition as per the BBD design. Figure 4 is the cross-section of the weld beads, from which the dimension of the penetration can be measured. These sections are obtained after grinding and etching with Kalling No. 2.

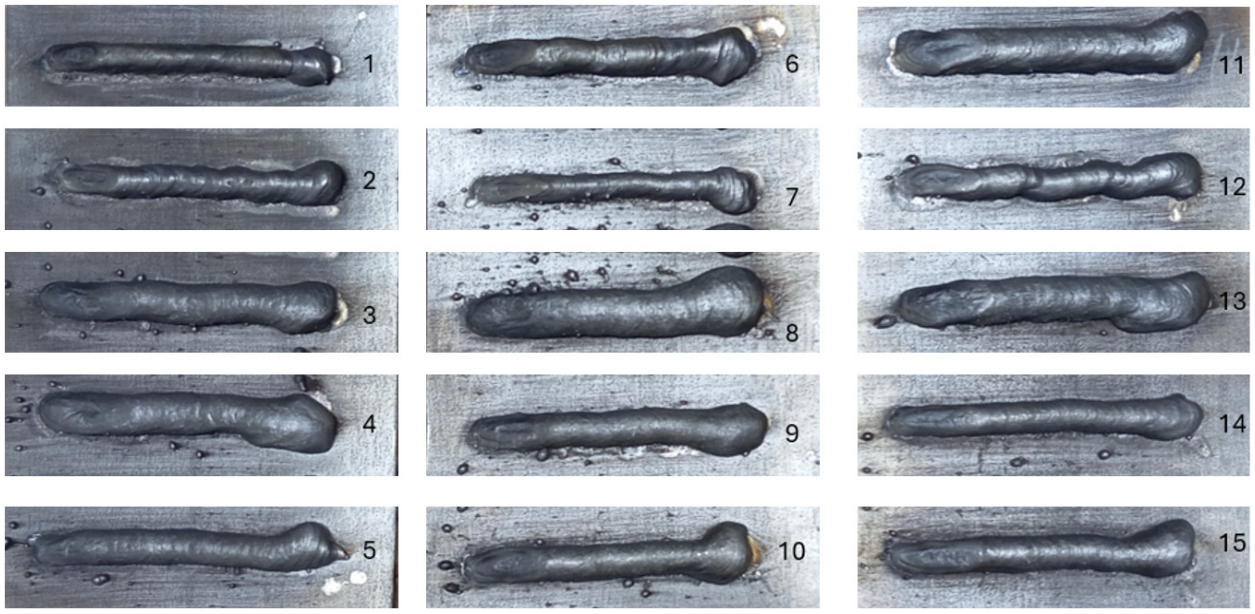

Figure 3. Welding bead for geometry measurement

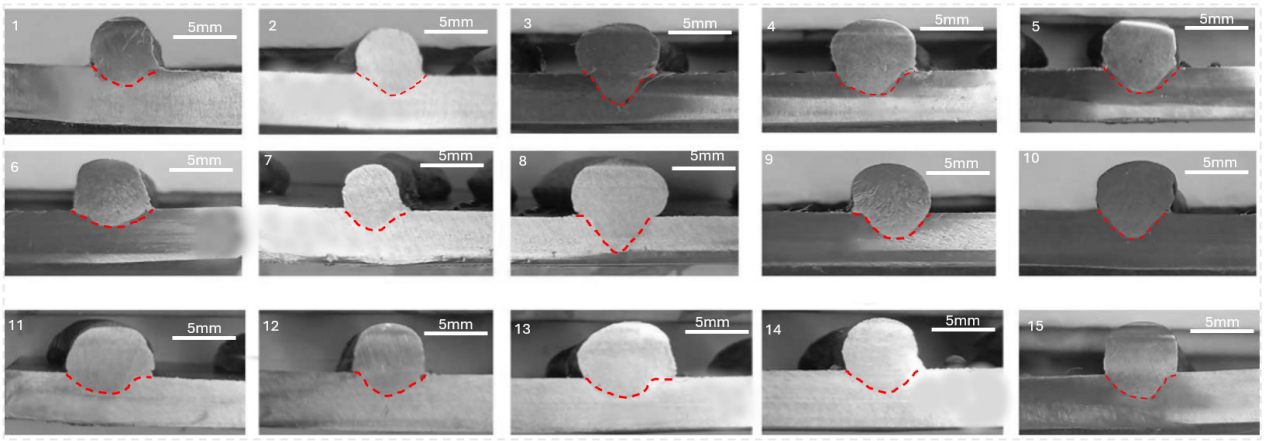

Figure 4. Cross section for weld beads

Table 4. Experimental values and predicted values using quadratic models

Run	Experimental values				Predicted values				Deviation			
	R (mm)	*W* (mm)	*R*/*W*	*P* (mm)	*R* (mm)	*W* (mm)	*R*/*W*	*P* (mm)	*R* (%)	*W* (%)	*R*/*W* (%)	*P* (%)
1	4.463	5.993	0.745	1.82	4.442	5.953	0.745	1.78	0.465	0.674	0	2.198
2	4.49	6.803	0.66	2.27	4.518	6.733	0.671	2.217	0.631	1.035	1.717	2.335
3	5.383	9.27	0.581	3.45	5.329	9.311	0.571	3.382	1.001	0.437	1.786	1.971
4	4.53	6.655	0.681	2.28	4.518	6.733	0.671	2.217	0.258	1.167	1.42	2.763
5	4.613	5.608	0.823	2.41	4.579	5.593	0.811	2.305	0.748	0.274	1.488	4.357
6	4.535	6.74	0.673	2.1	4.518	6.327	0.671	2.217	0.368	6.132	0.248	5.571
7	4.675	7.858	0.595	1.67	4.658	7.898	0.595	1.71	0.374	0.514	0	2.395
8	3.893	6.348	0.613	3.13	3.86	6.429	0.603	3.103	0.851	1.274	1.692	0.863
9	4.88	8.535	0.572	2.24	4.899	8.479	0.57	2.203	0.397	0.655	0.328	1.652
10	4.938	8.598	0.574	2.79	4.971	8.517	0.584	2.871	0.671	0.941	1.807	2.903
11	4.74	7.66	0.611	2.81	4.775	7.675	0.623	2.915	0.728	0.201	2.005	3.737
12	3.865	6.198	0.624	1.77	3.846	6.254	0.626	1.808	0.501	0.902	0.3	2.147
13	4.998	6.93	0.721	1.6	4.999	7.026	0.723	1.677	0.028	1.389	0.26	4.813
14	4.143	6.98	0.593	1.97	4.142	6.884	0.591	1.97	0.033	1.379	0.317	0.000
15	3.968	5.18	0.766	2.99	4.022	5.14	0.776	3.058	1.358	0.782	1.354	2.274

According to the fit summary, the quadratic model was selected as the fitting model for responses (*R*, *W*, *R*/*W* and *P*) and the corresponding regression equations are shown below:

$$\begin{aligned} R = {} & 7.56693 + 0.221117 \cdot Voltage - 0.017425 \cdot WFS + \\ & + 0.011697 \cdot TS + 0.000215 \cdot Voltage \cdot WFS + \\ & 0.001720 \cdot Voltage \cdot TS - 0.000105 \cdot WFS \cdot TS - \\ & - 0.009967 \cdot Voltage^2 + 0.000017 \cdot WFS^2 - \\ & - 0.002482 \cdot TS^2 \end{aligned} \quad (7)$$

$$\begin{aligned} W = {} & 14.00357 - 0.895427 \cdot Voltage + 0.040390 \cdot WFS \\ & - 0.0.957352 \cdot TS - 0.000583 \cdot Voltage \cdot WFS + \\ & + 0.004260 \cdot Voltage \cdot TS - 0.000270 \cdot WFS \cdot TS + \\ & 0.030147 \cdot Voltage^2 - 0.000014 \cdot WFS^2 + \\ & + 0.019947 \cdot TS^2 \end{aligned} \quad (8)$$

$$\begin{aligned} R/W = {} & 0.745663 + 0.092957 \cdot Voltage - \\ & 0.006836 \cdot WFS + 0.098347 \cdot TS + \\ & 0.000094 \cdot Voltage \cdot WFS - 0.000180 \cdot Voltage \cdot TS - \\ & 0.000017 \cdot WFS \cdot TS - 0.003787 \cdot Voltage^2 + \\ & + 4.58333E^{-06} \cdot WFS^2 - 0.002077 \cdot TS^2 \end{aligned} \quad (9)$$

$$\begin{aligned} P = {} & 19.04727 - 1.38589 \cdot Voltage - 0.000997 \cdot WFS \\ & - 0.467367 \cdot TS + 0.001730 \cdot Voltage \cdot WFS + \\ & + 0.038200 \cdot Voltage \cdot TS - 0.001435 \cdot WFS \cdot TS - \\ & - 0.004733 \cdot Voltage^2 - 9.5833E^{-07} \cdot WFS^2 + \\ & + 0.011817 \cdot TS^2 \end{aligned} \quad (10)$$

Based on the RSM models, the predicted values are calculated by Design Expert and listed in Table 4. The deviation of the experimental values and predictions are also presented.

4.2 Validation of the regression models

The above analysis shows that based on the experiment data, appropriate fitting models and regression equa–tions can be obtained. To validate the reliability of these models the ANOVA analysis is conducted using Design Expert 12.

The statistical analysis of the regression model for reinforcement is shown in Table 5, where the P-value is less than 0.0001 and the model is significant. The Lack of Fit F-value of 6.57 implies the Lack of Fit is not significant relative to the pure error. There is a 13.49% chance that a Lack of Fit F-value this large could occur due to noise. Non-significant lack of fit is superior.

Table 5. ANOVA for Quadratic model for Reinforcement (*R*)

Source	Sum of Squares	df	Mean Square	F-value	p-value	
Model	2.61	9	0.2903	109.84	< 0.0001	significant
A-Voltage	0.0017	1	0.0017	0.6256	0.4648	
B-WFS	0.1010	1	0.1010	38.23	0.0016	
C-TS	2.34	1	2.34	886.90	< 0.0001	
AB	0.0116	1	0.0116	4.37	0.0908	
AC	0.0018	1	0.0018	0.6997	0.4410	
BC	0.0110	1	0.0110	4.17	0.0965	
A²	0.0143	1	0.0143	5.42	0.0673	
B²	0.1026	1	0.1026	38.83	0.0016	
C²	0.0142	1	0.0142	5.38	0.0681	
Residual	0.0132	5	0.0026			
Lack of Fit	0.0120	3	0.0040	6.57	0.1349	not significant
Pure Error	0.0012	2	0.0006			
Cor Total	2.63	14				

Table 6. ANOVA for Quadratic model for Width (*W*)

Source	Sum of Squares	df	Mean Square	F-value	p-value	
Model	18.73	9	2.08	186.18	< 0.0001	significant
A-Voltage	0.0094	1	0.0094	0.8394	0.4016	
B-WFS	8.11	1	8.11	725.80	< 0.0001	
C-TS	9.30	1	9.30	832.12	< 0.0001	
AB	0.0850	1	0.0850	7.60	0.0400	
AC	0.0113	1	0.0113	1.01	0.3601	
BC	0.0729	1	0.0729	6.52	0.0510	
A^2	0.1311	1	0.1311	11.72	0.0188	
B^2	0.0738	1	0.0738	6.60	0.0501	
C^2	0.9182	1	0.9182	82.13	0.0003	
Residual	0.0559	5	0.0112			
Lack of Fit	0.0449	3	0.0150	2.71	0.2809	not significant
Pure Error	0.0110	2	0.0055			
Cor Total	18.79	14				

Table 7. ANOVA for Quadratic model for R/W ratio

Source	Sum of Squares	df	Mean Square	F-value	p-value	
Model	0.0841	9	0.0093	48.19	0.0003	significant
A-Voltage	0.0007	1	0.0007	3.63	0.1152	
B-WFS	0.0570	1	0.0570	293.75	< 0.0001	
C-TS	0.0027	1	0.0027	14.12	0.0132	
AB	0.0022	1	0.0022	11.39	0.0198	
AC	0.0000	1	0.0000	0.1044	0.7596	
BC	0.0003	1	0.0003	1.40	0.2893	
A^2	0.0021	1	0.0021	10.67	0.0223	
B^2	0.0078	1	0.0078	40.01	0.0015	
C^2	0.0100	1	0.0100	51.33	0.0008	
Residual	0.0010	5	0.0002			
Lack of Fit	0.0007	3	0.0002	2.21	0.3266	not significant
Pure Error	0.0002	2	0.0001			
Cor Total	0.0851	14				

Table 8. ANOVA for Quadratic model for Penetration (P)

Source	Sum of Squares	df	Mean Square	F-value	p-value	
Model	4.44	9	0.4931	34.64	0.0006	significant
A-Voltage	0.2312	1	0.2312	16.24	0.0100	
B-WFS	0.1458	1	0.1458	10.24	0.0240	
C-TS	0.0061	1	0.0061	0.4251	0.5432	
AB	0.7482	1	0.7482	52.57	0.0008	
AC	0.9120	1	0.9120	64.08	0.0005	
BC	2.06	1	2.06	144.68	< 0.0001	
A^2	0.0032	1	0.0032	0.2270	0.6538	
B^2	0.0003	1	0.0003	0.0238	0.8834	
C^2	0.3222	1	0.3222	22.64	0.0051	
Residual	0.0712	5	0.0142			
Lack of Fit	0.0507	3	0.0169	1.65	0.3987	not significant
Pure Error	0.0205	2	0.0102			
Cor Total	4.51	14				

Fit Statistics also show that the Predicted R^2 is 0.9259, which agrees with the Adjusted R^2 (0.9859). Therefore, this model can be used to navigate the design space. The statistical analysis of the regression model for Width is illustrated in Table 6, where the P-value is < 0.0001, which means the model is significant. The Lack of Fit F-value of 22.71 implies the Lack of Fit is not significant relative to the pure error. There is a 28.09% chance that a Lack of Fit F-value this large could occur due to noise. Non-significant lack of fit is good.

Fit Statistics show that the Predicted R^2 (0.9605) agrees with the Adjusted R^2 (0.9917), so this model can be used to navigate the design space.

The statistical analysis of the regression model for R/W is shown in Table 7, where the P-value is 0.0003 which means the model is significant. The Lack of Fit F-value of 2.21 implies the Lack of Fit is not significant relative to the pure error. There is a 32.66% chance that a Lack of Fit F-value this large could occur due to noise. Non-significant lack of fit is good.

Fit Statistics also show that the Predicted R^2 is 0.8540, which agrees with the Adjusted R^2 (0.9681), so this model can be used to navigate the design space.

The statistical analysis of the regression model for Penetration is shown in Table 8, where the P-value is 0.0006, which means the model is significant. The Lack of Fit F-value of 1.65 implies the Lack of Fit is not

significant relative to the pure error. There is a 39.87% chance that a Lack of Fit F-value this large could occur due to noise. Non-significant lack of fit is good.

The fit Statistics also show that the Predicted R^2 is 0.8099 which agrees with the Adjusted R^2 , which is 0.9558, so this model can be used to navigate the design space.

The above analysis shows that the four regression models obtained have been validated and can be used for subsequent prediction and optimization.

4.3 Effects of Welding Parameters

The RSM-BBD method not only obtains the relevant regression models but also obtains the effects of welding parameters on responses and the impact of the intersection and correlation of different parameters on the results, as shown in the following.

The response surface plots for the R , W , R/W, and P are shown in Figure 5 to Figure 8, demonstrating the effects of significant process parameters on bead geo–metry. Figure 5 shows the effects of each of the two in–put welding parameters (simultaneously) on Reinfor–cement. Figure 5(a) shows that Reinforcement increases significantly with the increase of WFS, while voltage has only a slight impact on the response. TS also has an influence on Reinforcement, as shown in Figure 5(b), and with the increase of TS, the Reinforcement decreases slightly. Figure 5(c) reveals that when considering WFS and TS together, the largest Reinforcement can be obtained in thetop-left of the plot with higher WFS and lower TS. On the contrary, the lowest reinforcement can be obtained for low WFS and higher TS.

The analysis indicates that voltage has a relatively minor influence on reinforcement height. In contrast, a higher WFS combined with a lower TS leads to significantly increased reinforcement, as shown in Figure 5(c). This is mainly attributed to the higher deposition rate and increased heat input resulting from elevated WFS, which promotes greater accumulation of molten material. At the same time, a lower TS reduces the heat dissipation per unit length, allowing more filler metal to solidify on the surface before the pool moves forward. These combined effects contribute to the formation of a higher reinforcement.

Figure 6 shows the effects of each two input welding parameters (simultaneously) on the Width. Figure 6(a) shows that width increases significantly with the increase of WFS, while voltage has only a slight impact on the response. TS also has an influence on Width, as shown in Figure 6(b), and with the increase of TS, the Width decreases. Figure 6(c) reveals that when considering WFS and TS together, the largest Width can be obtained in the top-right of the plot with higher WFS and lower TS. On the contrary, the lowest width can be obtained for low WFS and higher TS.

The observed trends can be explained by the effects of the welding parameters on arc behavior and molten pool dynamics. Bead width is primarily governed by arc spreading and the lateral flow of molten metal. Higher WFS leads to higher heat input, enlarging the molten pool and allowing the bead to spread further, thus increasing the width. Conversely, a higher travel speed reduces the residence time of the arc on the substrate, limiting lateral spreading and resulting in a narrower bead.

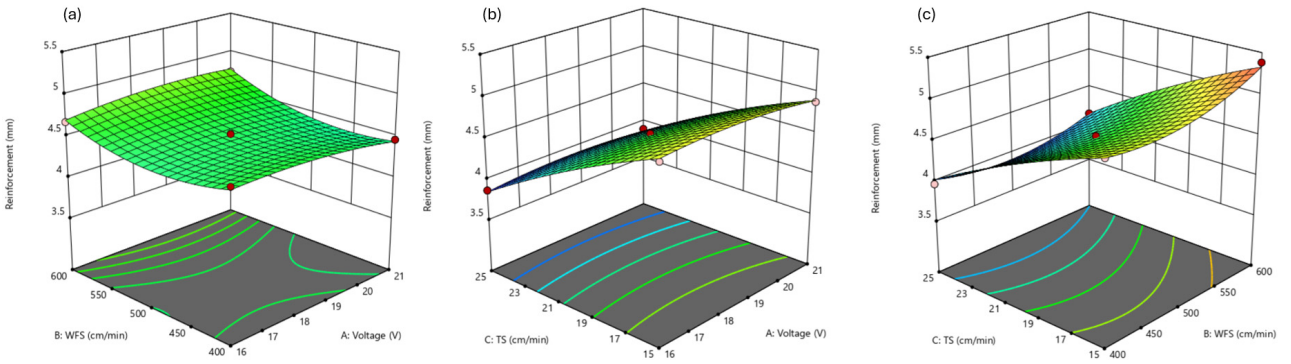

Figure 5. The response surface plots for Reinforcement: (a) factors of Voltage and WFS, (b) factors of Voltage and TS, (c) factors of WFS and TS

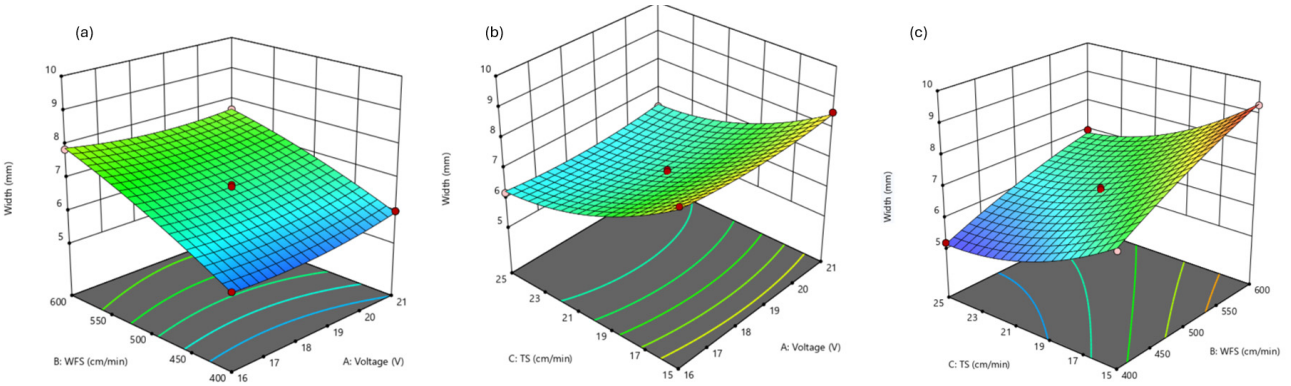

Figure 6. The response surfaces plots for Width: (a) factors of Voltage and WFS, (b) factors of Voltage and TS, (c) factors of WFS and TS

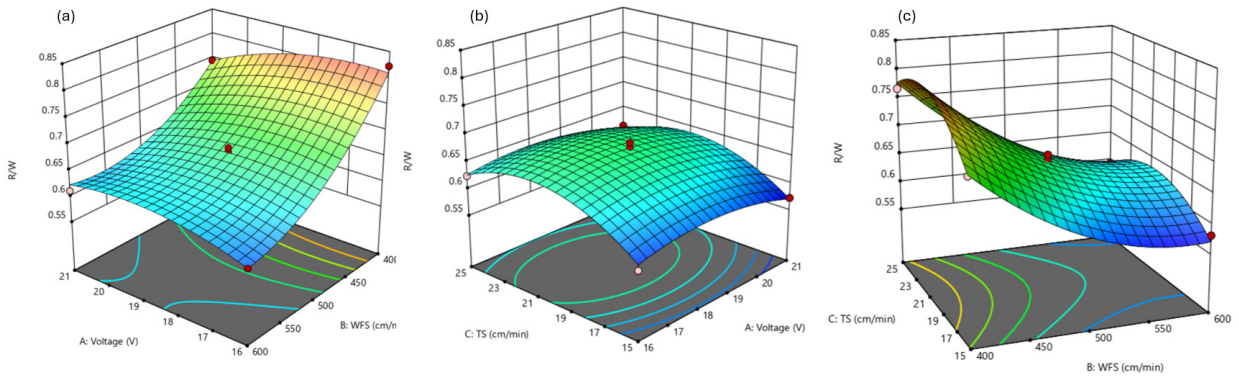

Figure 7. The response surface plots for R/W: (a) factors of Voltage and WFS, (b) factors of Voltage and TS, (c) factors of WFS and TS

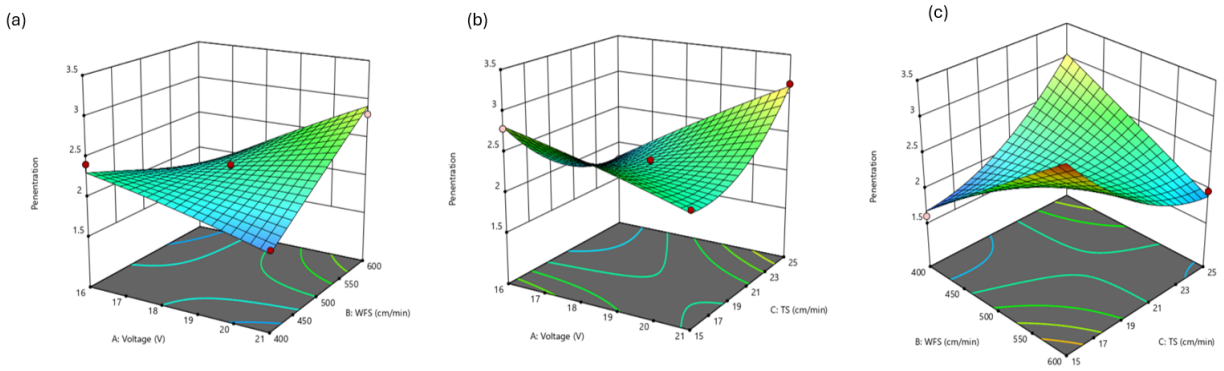

Figure 8. The response surface plots for penetration: (a) factors of Voltage and WFS, (b) factors of Voltage and TS, (c) factors of WFS and TS

Figure 7 shows the effects of each of the two input welding parameters (simultaneously) on the aspect ratio *R*/*W*. Figure 7(a) shows that there is a higher value for *R*/*W* when both WFS and Voltage are lower; WFS can influence *R*/*W* significantly, with the increase of voltage, *R*/*W* increases slightly. Figure 7(b) reveals that there is a maximum value when both TS and voltage are in there middle values (TS of 20 cm/min and voltage of 18.5 V). Figure 7(c) displays that when considering WFS and TS together, the largest *R*/*W* can be obtained in the top-left of the plot with lower WFS and higher TS. On the contrary, the lowest R/W can be obtained for low WFS and higher TS.

The results showed that although WFS increased reinforcement height, the bead width exhibited a more significant rise. The enhanced heat input and filler metal volume at higher WFS likely promoted greater molten pool spreading rather than vertical buildup. Similar observations have been reported where excessive heat input led to broader, flatter beads due to increased molten metal flow and arc spreading [42].

Figure 8 shows the effects of each of the two input welding parameters (simultaneously) on the Penetration. Figure 8(a) shows a higher value for *P* when both WFS and Voltage are lower; WFS can influence *P* signi–ficantly, with the increase of voltage *P* increasing slig–htly. Figure 8(b) reveals that there is a maximum value when both TS and voltage are highest. Figure 8(c) disp–lays that when considering WFS and TS together, the largest P can be obtained with higher WFS and lower TS.

The underlying trends can be further understood by studying the thermal and physical mechanisms that control weld pool behavior and penetration. Penetration is closely related to heat input and arc energy concen–tration. Higher wire width (WFS) increases the total heat input, thereby enhancing base metal melting and penetration. On the other hand, increasing wire travel speed reduces the heat input per unit length, limiting the time available for heat transfer and reducing penet–ration. Higher voltage may cause the arc to be diffuse and less focused, which may slightly reduce penetration, depending on arc stability and current density distribution.

The above analysis shows that three parameters (Voltage, WFS, and TS) have significant impacts on different single responses (*R*, *W*, *R*/*W*, and *P*), and single-objective optimization can be obtained. However, *R*, *W*, *R*/*W*, and *P* need to be considered comprehen–sively in the subsequent AM process, so multi-objective optimi–zation is required based on the above prediction results.

4.4 GRA application

Based on above describe models, 100 solutions are predicted, and then the GRA algorithm mentioned in section 2.3.2 is applied for multi-objective optimization. Table 9 shows the results of the Top10 solutions according to the GRA analysis, where GRG order will be applied to determine the optimal parameters. As in the system analyzed, it is expected that the *R* and *R*/*W* values are higher and the *W* value is lower. While calculating the GRG values presented in Table 10, values (*R*, *W*, *R*/*W* and *P*) were normalized using (2) or (3), respectively. Then, (4) is used to calculate the GRC value. Finally, (5) is used to calculate the value of GRG, and then the GRG order is shown.

Table 9. Top 10 parameters according to GRG order

Run	Welding parameters				Responses			GRC				GRG	GRG Order
	Voltage	WFS	TS	R	W	R/W	P	R	W	R/W	P		
73	16.783	403.231	24.862	4.032	5.109	0.785	2.843	0.689	1.000	0.652	0.276	0.654273	1
2	18.5	400	25	4.022	5.139	0.776	3.058	0.700	0.964	0.582	0.250	0.624163	2
8	16	400	20	4.579	5.593	0.811	2.305	0.359	0.623	1.000	0.373	0.58866	3
43	16.312	557.078	24.586	3.981	6.766	0.587	1.367	0.753	0.325	0.179	0.953	0.55261	4
11	16	500	25	3.846	6.254	0.626	1.808	1.000	0.411	0.209	0.550	0.542444	5
44	18.46	409.011	21.101	4.443	5.51	0.79	2.24	0.408	0.666	0.699	0.389	0.540441	6
86	16.093	563.888	23.223	4.172	6.973	0.597	1.355	0.558	0.300	0.186	0.973	0.504084	7
18	16.985	575.675	24.665	4.052	6.832	0.587	1.456	0.666	0.317	0.179	0.831	0.498115	8
26	18.207	412.835	19.22	4.63	5.894	0.778	2.038	0.344	0.504	0.597	0.451	0.473925	9
75	18.791	427.364	21.926	4.316	5.644	0.755	2.352	0.467	0.599	0.466	0.362	0.473176	10

The largest value is determined as the best experimental parameter for the system. Based on the results in Table 9, the 73th run has the optimal results for the following research, which means that the welding parameters of voltage (16.783 V), WFS (403.231 cm/min) and TS (24.862 cm/min) are choosen as the parameters in the next step of the research.

5. VALIDATION

To verify the reliability of the optimal results, additive manufacturing processes were carried out using the optimal parameters obtained in section 3. The ten-layer 3D structural wall is shown in Figure 9. The average height is 31.25 mm, and the average width is 5.2 mm. The appearance of the wall is fine and the layers are parallel to each other at even heights. The boundaries between layers are tightly bonded, without obvious defects such as gaps and weld leaks. The fabricated walls exhibit high vertical uniformity, with no significant deviation in thickness along the build height.

The results reveal that using the optimal parameters can obtain the acceptable 3D structural walls, and the parameters can be applied in the following additive manufacturing studies.

Figure 9. Multi-layers 3D structure wall using the optimal parameters

6. CONCLUSION

To obtain the optimal parameters for the additive manufacturing process, Response surface methodology (RSM) - Box-Behnken design (BBD) and Grey relational analysis (GRA) methodologies are utilized. The conclusions include:

- Based on the BBD design of the experiment method, model, and ANOVA analysis, the impact of each parameter is obtained. Among them, TS had more influence than the other two parameters both in terms of R and W.
- With the increase of WFS and decrease of TS, reinforcement and bead width values are increasing. The two responses have similar trends.
- Voltage is the least important factor for all responses, i.e., *R*, *W*, *R*/*W*, and *P*.
- Regression equations from RSM show significance for all responses, which can verify the reliability of the model.
- The GRA method is applied to the 100 solutions with the given weight of three responses, providing optimized welding parameters: voltage of 16.783 V, WFS of 403.231 cm/min, and TS of 24.862 cm/min.
- Validation for multi-layer single pass 3D AM structure shows that using optimization results can ensure an excellent welding appearance.

The results from this paper can provide a reliable reference for the following study on the additive manufacturing process. It can ensure that each weld bead can obtain an acceptable appearance and the accumulation can be realized at an efficient speed.

REFERENCES

[1] Int, A.: Standard terminology for additive manufacturing technologies, 2013.

[2] Güden, S., Motorcu, A.R., Yazici, M.: Examining and Optimizing the Weld Area and Mechanical Performance of Thermoplastic Parts Manufactured by Additive Manufacturing and Welded by Friction Stir Welding. FME Transactions, Vol. 52, No. 2, pp. 279-294, 2024.

[3] Kumar, M.D.B. et al.: Effect of Post-Fabrication Treatments on Surface Residual Stresses of Additive Manufactured Stainless Steel 316L. FME Transactions, Vol. 49, No. 1, pp. 87-94, 2021.

[4] Zhang, D., Liu, A., Yin, B., Wen, P.: Additive manufacturing of duplex stainless steels - A critical review, J. Manuf. Process., Vol. 73, pp. 496-517, 2022.

[5] Bártová, K., Bárta, J., Ptačinová, J.: Study of multilayer welded structure made of AISI 316LSi using WAAM, Tehnički vjesnik, Vol. 31, No. 2, pp. 574-578, 2024.

[6] Šket, K., Brezočnik, M., Karner, T., Balšak, R., Ficko, M., Vuherer, T., Gotlih, J.: Predictive modelling of weld bead geometry in wire arc additive

manufacturing, J. Manuf. Mater. Process., Vol. 9, No. 2, pp. 67, 2025.

[7] Novak, R., Valjak, F., Bojčetić, N., Šercer, M.: Design principle for additive manufacturing: Direct metal sintering, Tehnički vjesnik, Vol. 30, No. 3, pp. 937-944, 2023.

[8] Wang, W.L., Guo, M., Liu, J., Wang, Y., Li, H.: A review of the melt structure and crystallization behavior of non-reactive mold flux for the casting of advanced high-strength steels, Steel Res. Int., Vol. 93, No. 3, 2022.

[9] Palanisamy, C., Raman, R., Dhanraj, P.K.: Additive manufacturing: A review on mechanical properties of PolyJet and FDM printed parts, Polym. Bull., Vol. 79, No. 9, pp. 7065-7116, 2022.

[10] Pacifici, A., Polimeni, A., Pacifici, L.: Additive manufacturing and biomimetic materials in oral and maxillofacial surgery: A topical overview, J. Biol. Regul. Homeost. Agents, Vol. 32, No. 6, pp. 1579-1582, 2018.

[11] Gong, X.B., Anderson, T. Chou, K.: Review on powder-based electron beam additive manufac–turing technology, in: Proc. ASME/ISCIE Int. Symp. Flexible Automation (ISFA 2012), 2013, pp. 507-515.

[12] Xia, C.Y., Pan, Z., Polden, J., Li, H., Xu, Y., Chen, S., Zhang, Y.: A review on wire arc additive manu–facturing: Monitoring, control and a framework of automated system, J. Manuf. Syst., Vol. 57, pp. 31-45, 2020.

[13] Wallich, P.: 3-D printers proliferate, IEEE Spec–trum, Vol. 47, No. 9, pp. 23, 2010.

[14] Gisario, A., Kazarian, M., Martina, F., Mehrpouya M.: Metal additive manufacturing in the commer–cial aviation industry: A review, J. Manuf. Syst., Vol. 53, pp. 124-149, 2019.

[15] Haden, C.V., Zeng, G., Carter, F.M., Ruhl, C., Krick, B.A., Harlow, D.G.: Wire and arc additive manufactured steel: Tensile and wear properties, Addit. Manuf., Vol. 16, pp. 115-123, 2017.

[16] Wang, H.F., Klaric, S., Havrlisan, S.: Preliminary Study of Bead-On-Plate Welding Bead Geometry for 316L Stainless Steel Using GMAW. FME Transactions, Vol. 52, No. 4, pp. 563-572, 2024.

[17] Yuan, Y.H. et al.: Expe–rimental and numerical investigation of CMT wire and arc additive manufacturing of 2205 duplex stainless steel, Coatings, Vol. 12, No. 12, pp. 1971, 2022.

[18] Ettefagh, A.H., Guo, S.M., Raush, J.: Corrosion performance of additively manufactured stainless steel parts: A review, Addit. Manuf., Vol. 37, 2021.

[19] Hosseini, V. A., Högström, M., Hurtig, K., Valiente Bermejo, M. A., Stridh, L.-E., Karlsson, L.: Wire-arc additive manufacturing of a duplex stainless steel: Thermal cycle analysis and microstructure characterization, Weld. World, Vol. 63, No. 4, pp. 975-987, 2019.

[20] Huang, X., Kwok, C. T., Niu, B., Luo, J., Zou, X., Cao, Y., Yi, J., Pan, L., Qiu, W., Zhang, X.: Anisotropic behavior of super duplex stainless steel fabricated by wire arc additive manufacturing, J. Mater. Res. Technol., Vol. 27, pp. 1651-1664, 2023.

[21] Kannan, A. R., Siva Shanmugam, N., Devendranath Ramkumar, K., Rajkumar, V.: Studies on super duplex stainless steel manufactured by wire arc additive manufacturing, Trans. Indian Inst. Met., Vol. 74, No. 7, pp. 1673-1681, 2021.

[22] Rajesh Kannan, A., Siva Shanmugam, N., Raj–kumar, V., Vishnukumar, M.: Insight into the mic–rostructural features and corrosion properties of wire arc additive manufactured super duplex stain–less steel (ER2594), Mater. Lett., Vol. 270, 2020.

[23] Zhang, Y.Q., Cheng, F.J., Wu, S.J.: Improvement of pitting corrosion resistance of wire arc additive manufactured duplex stainless steel through post-manufacturing heat-treatment, Mater. Charact., Vol. 171, 2021.

[24] Kumar, P., Maji, K.: Experimental investigations and parametric effects on depositions of super duplex stainless steel in wire arc additive manufac–turing, Proc. Inst. Mech. Eng. Part E J. Process Mech. Eng., 2023.

[25] Miranda-Pérez, A.F., Rodríguez-Vargas, B.R., Calliari, I. and Pwzzato, L.: Corrosion resistance of GMAW duplex stainless steels welds, Materials, Vol. 16, No. 5, pp. 1847, 2023.

[26] Zhang, Y.Q., Wu, S.J. and Cheng, F.J.: A duplex stainless steel (DSS) with striking tensile strength and corrosion resistance produced through wire arc-additive manufacturing (WAAM) using a newly developed flux-cored wire, Mater. Lett., Vol. 313, 2022.

[27] Knezović, N., Garašić, I., Jurić, I.: Influence of the interlayer temperature on structure and properties of wire and arc additive manufactured duplex stain–less steel product, Materials, Vol. 13, No. 24, 2020.

[28] Chaudhari, R., Parmar, H., Vora, J., Patel, V.K.: Parametric study and investigations of bead geo–metries of GMAW-based wire-arc additive manu–facturing of 316L stainless steels, Metals, Vol. 12, No. 7, 2022.

[29] Kumar, A., Maji, K.: Selection of process para–meters for near-net shape deposition in wire arc additive manufacturing by genetic algorithm, J. Mater. Eng. Perform., Vol. 29, No. 5, pp. 3334-3352, 2020.

[30] Zhao, Y.T., Li, W.G., Liu, A.: Optimization of ge–ometry quality model for wire and arc additive manufacture based on adaptive multi-objective grey wolf algorithm, Soft Comput., Vol. 24, No. 22, pp. 17401-17416, 2020.

[31] Vora, J. et al.: Optimization of bead morphology for GMAW-based wire-arc additive manufacturing of 2.25 Cr-1.0 Mo steel using metal-cored wires, Appl. Sci. Basel, Vol. 12, No. 10, 2022.

[32] Chaudhari, R., Bhatt, R., Vaghasia, V., Raja, D.B., Patel, V.K., Khanna, S., Vora, J., Patel, V.V.: A parametric study and experimental investigations of

microstructure and mechanical properties of multi-layered structure of metal core wire using wire arc additive manufacturing, J. Adv. Joining Process., Vol. 8, 2023.

[33] Acherjee, B., Prakash, S., Kuar, A.S., Mitra, S.: Grey relational analysis based optimization of under–water Nd:YAG laser micro-channeling on PMMA, in: 12th Global Congress on Manufacturing and Management (GCMM 2014), 2014, Vol. 97, pp. 1406-1415.

[34] Sultzer, J., Totzauer, T, Wittig, B., Zinke, M., Jüttner, S.: GMAW cold wire technology for adjus–ting the ferrite-austenite ratio of wire and arc addi–tive manufactured duplex stainless steel compo–nents, Metals, Vol. 9, No. 5, 2019.

[35] Behbahani, M., Moghaddam, M.R.A., Arami, M.: Techno-economical evaluation of fluoride removal by electrocoagulation process: Optimization thro–ugh response surface methodology, Desalination, Vol. 271, No. 1-3, pp. 209-218, 2011.

[36] Nóbrega, G., Souza, M.S., Rodriguez-Martin, M., Rodriguez-Gonzalvez, P., Ribeiro, J.: Parametric optimization of the GMAW welding process in thin thickness of austenitic stainless steel by Taguchi method, Appl. Sci. Basel, Vol. 11, No. 18, 2021.

[37] Akgül, V., Kursuncu, B., Kaya, H.: Response surface methodology-based multi-objective grey relation optimization for impinging jet cooling with Al□O□ /water nanofluid on a curved surface, Neural Com–put. Appl., Vol. 35, No. 19, pp. 13999-14012, 2023.

[38] Zhao, Z., Chen, W., Xie, X., Ma, T., Huang, S., Xiao, J., Liang, Z.: Wear resistance of Cronidur 30 steel enhanced by optimizing the strengthened grinding process (SGP) parameters using a Box-Behnken design (BBD) method, J. Manuf. Process., Vol. 122, pp. 7-20, 2024.

[39] Mora, J.M.R. et al.: Biodiesel production from soybean oil via LiOH-pumice catalytic transes–terification and BBD-RSM optimization, Energy Rep., Vol. 11, pp. 4032-4043, 2024.

[40] Ghabi, W., Landolsi, K., Echouchene, F., Bajahzar, A., Msaddek, M., Belmabrouk, H.: Optimizing synthesis and catalytic performance of novel β-keto-enamine complexes of Ni(II) using BBD design and PSO-ANN, Inorg. Chim. Acta, Vol. 574, 2025.

[41] Bestard, G.A., Alfaro, S.C.A.: Measurement and estimation of the weld bead geometry in arc wel–ding processes: The last 50 years of development, J. Braz. Soc. Mech. Sci. Eng., Vol. 40, No. 9, 2018.

[42] DebRoy, T. et al.: Additive manufacturing of meta–llic components - Process, structure and properties. Progress in Materials Science, Vol. 92, pp. 112-224, 2018.

NOMENCLATURE

AM	additive manufacturing
GMAW	gas metal arc welding
WFS	wire feed speed
TS	travel speed
ANOVA	analysis of variance
GRA	Grey relational analysis
BBD	Box-Behnken design
RSM	response surface methodology
R	reinforcement
R/W	ratio of weld reinforcement to width
W	width
P	penetration

ИСТРАЖИВАЊЕ ГЕОМЕТРИЈЕ НАВАРА ДУПЛЕКС ЧЕЛИКА КОД АДИТИВНЕ ПРОИЗВОДЊЕ ПРИМЕНОМ МИГ ПОСТУПКА ЗАВАРИВАЊА

Х. Ванг, Ш. Кларић, С. Хаврлишан

Применом процеса адитивне производње (АМ) електролучним заваривањем тањивом жицом у заш–тити инертног гаса (МИГ) при производњи компо–ненти од дуплех нерђајућег челика може се смањити отпад материјала, те омогућити контрола микро–структуре и хемијског састава легуре у различитим деловима производа кроз пажљив одабир и контролу параметара заваривања. Међутим, будући да је потребно ускладити постизање веће количине депозита, већег надвишења навара и пенетрације те мање ширине навара, једноставно постављање параметара заваривања не мора увек дати жељене резултате. стога је циљ овог истраживања анали–зирати утицај напона, брзине извлачења жице (wfs) и брзине помака (ts) како би се експерименталним методама одредиле оптималне вриједности параметара. За вишекритеријумску оптимизацију коришћена је Grey relational analysis (GRA), чиме су добивени оптимални параметри: напон (16,783 В), брзина извлачења жице (403,231 cm/min) и брзина помака (24,862 cm/min). ови параметри примењени су за израду ам зида од 10 слојева, при чему је постигнуто стабилно понашање лука, добра међуслојна веза и уједначена морфологија зида.